


## AUTHOR QUERY FORM

	<p><b>Journal:</b> Appl. Phys. Lett.</p> <p><b>Article Number:</b> 076431APL</p>	<p>Please provide your responses and any corrections by annotating this PDF and uploading it according to the instructions provided in the proof notification email.</p>
---	---	--

Dear Author,

Below are the queries associated with your article; please answer all of these queries before sending the proof back to AIP. Please indicate the following:

Figures that are to appear as color online only (i.e., Figs. 1, 2, 3) \_\_\_\_\_ (this is a free service).  
 Figures that are to appear as color online and color in print \_\_\_\_\_ (a fee of \$325 per figure will apply).

**Article checklist:** In order to ensure greater accuracy, please check the following and make all necessary corrections before returning your proof.

1. Is the title of your article accurate and spelled correctly?
2. Are the author names in the proper order and spelled correctly?
3. Please check affiliations including spelling, completeness, and correct linking to authors.
4. Did you remember to include acknowledgment of funding, if required, and is it accurate?

Location in article	Query / Remark: click on the Q link to navigate to the appropriate spot in the proof. There, insert your comments as a PDF annotation.
<a href="#">AQ1</a> <a href="#">AQ2</a> <a href="#">AQ3</a> <a href="#">AQ4</a> <a href="#">AQ5</a>	<p>Sections headings are not allowed in APL. Therefore, all headings have been deleted throughout the article.</p> <p>Please provide publisher name in Ref. 17.</p> <p>Please provide page number in Refs. 5, 7, and 21.</p> <p>Please verify the change in page number in Ref. 10.</p> <p>We were unable to locate a digital object identifier (doi) for Ref. 20. Please verify and correct author names and journal details (journal title, volume number, page number, and year) as needed and provide the doi. If a doi is not available, no other information is needed from you. For additional information on doi's, please select this link: <a href="http://www.doi.org/">http://www.doi.org/</a>.</p>

Thank you for your assistance.

# 1 A strained silicon cold electron bolometer using Schottky contacts

2 T. L. R. Brien,<sup>1,a)</sup> P. A. R. Ade,<sup>1</sup> P. S. Barry,<sup>1</sup> C. Dunscombe,<sup>1</sup> D. R. Leadley,<sup>2</sup> D. V. Morozov,<sup>1</sup>  
 3 M. Myronov,<sup>2</sup> E. H. C. Parker,<sup>2</sup> M. J. Prest,<sup>2</sup> M. Prunnila,<sup>3</sup> R. V. Sudiwala,<sup>1</sup> T. E. Whall,<sup>2</sup>  
 4 and P. D. Mauskopf<sup>1,4</sup>

5 <sup>1</sup>*School of Physics and Astronomy, Cardiff University, Queen's Buildings, The Parade, Cardiff CF24 3AA,*  
 6 *United Kingdom*

7 <sup>2</sup>*Department of Physics, University of Warwick, Coventry CV4 7AL, United Kingdom*

8 <sup>3</sup>*VTT Technical Research Centre of Finland, P.O. Box 1000, FI-02044 VTT Espoo, Finland*

9 <sup>4</sup>*Department of Physics and School of Earth and Space Exploration, Arizona State University,*  
 10 *650 E. Tyler Mall, Tempe, Arizona 85287, USA*

11 (Received 20 May 2014; accepted 23 July 2014; published online xx xx xxxx)

12 We describe optical characterisation of a Strained Silicon Cold Electron Bolometer (CEB),  
 13 operating on a 350 mK stage, designed for absorption of millimetre-wave radiation. The silicon cold  
 14 electron bolometer utilises Schottky contacts between a superconductor and an  $n^{++}$  doped silicon  
 15 island to detect changes in the temperature of the charge carriers in the silicon, due to variations in  
 16 absorbed radiation. By using strained silicon as the absorber, we decrease the electron-phonon cou-  
 17 pling in the device and increase the responsivity to incoming power. The strained silicon absorber is  
 18 coupled to a planar aluminium twin-slot antenna designed to couple to 160 GHz and that serves as  
 19 the superconducting contacts. From the measured optical responsivity and spectral response, we cal-  
 20 culate a maximum optical efficiency of 50% for radiation coupled into the device by the planar  
 21 antenna and an overall noise equivalent power, referred to absorbed optical power, of  $1.1 \times$   
 22  $10^{-16} \text{ W Hz}^{-1/2}$  when the detector is observing a 300 K source through a 4 K throughput limiting  
 23 aperture. Even though this optical system is not optimized, we measure a system noise equivalent  
 24 temperature difference of  $6 \text{ mK Hz}^{-1/2}$ . We measure the noise of the device using a cross-  
 25 correlation of time stream data measured simultaneously with two junction field-effect transistor  
 26 amplifiers, with a base correlated noise level of  $300 \text{ pV Hz}^{-1/2}$  and find that the total noise is consist-  
 27 ent with a combination of photon noise, current shot noise, and electron-phonon thermal noise.

© 2014 AIP Publishing LLC. [<http://dx.doi.org/10.1063/1.4892069>]

AQ1 28 Photon noise limited detection of millimetre-wave radia-  
 29 tion has been demonstrated with a number of cryogenic  
 30 detectors such as: semiconductor bolometers, transition edge  
 31 sensors, and kinetic inductance detectors.<sup>1,2</sup> A bolometer  
 32 consists of a thermally isolated absorber that converts  
 33 absorbed radiation into thermal energy, which is detected by  
 34 means of a sensitive thermometer. The concept of using the  
 35 weak coupling between electrons and phonons at low tem-  
 36 peratures, combined with a normal metal-insulator-supercon-  
 37 ductor (NIS) tunnel junction thermometer, to make a fast and  
 38 sensitive hot electron bolometer, was first proposed by  
 39 Nahum, Richards, and Mears.<sup>3,4</sup> Dual normal metal-insula-  
 40 tor-superconductor (SINIS) junctions, coupled to an absorb-  
 41 ing metallic island, can be used to simultaneously act as a  
 42 microrefrigerator by extracting heat from the electrons and  
 43 as a bolometric detector. The wavelengths that the island  
 44 absorbs can be defined by patterning the superconducting  
 45 leads into an antenna.

46 Schmidt *et al.*<sup>5</sup> describe how the use of a combined  
 47 microwave and DC biasing signal, along with frequency do-  
 48 main multiplexing techniques, can be used to realise large  
 49 imaging arrays (up to  $10^5$  pixels) of Cold Electron  
 50 Bolometers (CEBs).

51 Detailed calculations of the characteristics of these  
 52 CEBs indicate that they should exhibit a combination of fast  
 53 response speeds ( $< 1 \mu\text{s}$ ) and high sensitivity. Achieving high

sensitivities with metal-based cold electron bolometers 54  
 requires fabrication of submicron metal islands. 55

56 Replacing the normal metal with a degenerately doped  
 57 silicon offers reduced electron-phonon coupling compared to  
 58 standard metals and thus gives higher sensitivity for a given  
 59 island volume.<sup>6</sup> It has been proposed<sup>7</sup> that using a strained  
 60 silicon absorber enables fabrication of detectors with photon  
 61 noise limiting sensitivity using standard photolithographic  
 62 techniques. Initial reports of optical noise equivalent power  
 63 (NEP) for metal based cold electron bolometers have been  
 64 published in recent years.<sup>8,9</sup> Most of these measurements  
 65 have been based on radiation absorbed from a cold black-  
 66 body source, this does not allow for the spectral response of  
 67 the detector to be studied. They have also all reported optical  
 68 noise equivalent powers limited by the readout electronics.  
 69 Here, we present optical measurements of a strained silicon  
 70 cold electron bolometer designed to absorb millimetre-wave  
 71 radiation, these measurement have been taken with the de-  
 72 tector looking out of a window in the cryostat which allowed  
 73 for a number of sources, including a Fourier transform spec-  
 74 trometer, to be observed.

75 The electrothermal properties of both the normal metal-  
 76 insulator-superconductor and the symmetric (SINIS) struc-  
 77 tures have been well studied.<sup>3,4,10–13</sup> Fig. 1 shows a typical  
 78 normal metal-insulator-superconductor structure (shown in  
 79 the presence of an external bias such that  $eV = \Delta$ ). These  
 80 devices have been shown<sup>13</sup> to be able to reduce electron tem-  
 81 perature from 300 mK to below 100 mK. For a sensitive

<sup>a)</sup>Electronic mail: tom.brien@astro.cf.ac.uk

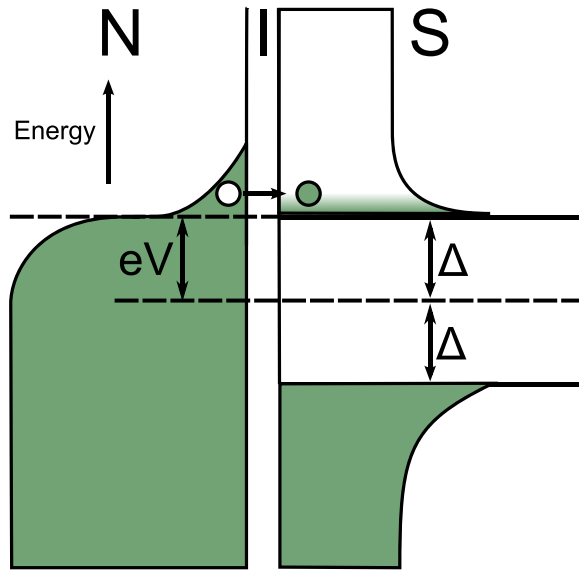


FIG. 1. Energy bands for a biased normal metal-insulator-superconductor NIS structure. In order for electrons to tunnel from the normal metal (left) into the superconductor (right), we require that  $eV > \Delta - k_B T_e$ , where  $V$  is the voltage across the structure due to the bias,  $T_e$  is the electron temperature, and  $\Delta$  is half the superconducting gap.

bolometric detector, we would like the absorber (the normal metal in this case) to have as small a volume as possible.

A similar structure, superconductor-semiconductor-superconductor (SSmS), exists where the normal metal is replaced by a doped semiconductor and the insulator replaced by a Schottky contact formed between the semiconductor and the superconductor.<sup>12</sup> These devices have the advantage of decreased electron-phonon coupling compared to the normal metal based type of device<sup>7</sup> and reduced electron density. The current,  $I$ , flowing through each of the symmetric junctions is given by

$$I = \frac{1}{eR_N} \int_{\Delta}^{\infty} \frac{E}{\sqrt{E^2 - \Delta^2}} \times [f(E - eV/2, T_e) - f(E + eV/2, T_e)] dE, \quad (1)$$

where  $R_N$  is the normal-state resistance due to tunnelling through the insulating barrier,  $\Delta$  is half the superconducting bandgap,  $V$  is the voltage across the structure, and  $f(E, T)$  is the Fermi distribution for electrons at temperature  $T_e$ . Associated with this current is a flow of heat from the central island which dissipates a power,  $P$ , within the device of

$$P = IV + \frac{2}{e^2 R_N} \int_{\Delta}^{\infty} \frac{E^2}{\sqrt{E^2 - \Delta^2}} \times [2f(E, T_s) - f(E - eV/2, T_e) - f(E + eV/2, T_e)] dE. \quad (2)$$

This power is bias dependent and is negative (cooling) for bias voltages  $eV \lesssim 3\Delta$ .

In a cold electron bolometer, when the absorber is heated by incident optical power, it is this cooling power, associated with the most energetic of charges tunnelling out of the absorber, which removes the heat. Since the cooling (thermal resetting) of the bolometer is carried out directly by electron diffusion (as opposed to the long, weak, thermal links required by many of today's most sensitive

bolometers<sup>14–16</sup>), the thermal time constant associated with the cold electron bolometer is governed by the tunnelling time. This can be<sup>17</sup> as low as 10 ns, whereas other types of detector<sup>18</sup> have response times of the order of 1 ms.

In addition to this cooling power, the electrons are also heated or cooled by the weak thermal link to the phonons. This heating term,  $P_{e-ph}$ , is given by

$$P_{e-ph} = \Sigma \Omega (T_e^\beta - T_{ph}^\beta), \quad (3)$$

where  $\Sigma$  is a material constant that has been measured<sup>19</sup> to be  $2 \times 10^7 \text{ W K}^{-6} \text{ m}^{-3}$ ;  $\Omega$  is the volume of the bolometer's absorber;  $T_{ph}$  and  $T_e$  are the phonon and electron temperatures, respectively, and the power  $\beta$  has been found<sup>19</sup> to be 6. From this, we can define a thermal conductance,  $G$ , from the phonons to the electrons as

$$G = \frac{dP}{dT_e} = \beta \Sigma \Omega T_e^{\beta-1}. \quad (4)$$

The total NEP for the cold electron bolometer is comprised of several terms and has been fully derived by Golubev and Kuzmin<sup>20</sup> to be

$$NEP_{CEB}^2 = \frac{\langle \delta V^2 \rangle_{\text{amp}}}{S^2} + 2\beta k_B \Sigma \Omega (T_e^{\beta+1} + T_{ph}^{\beta+1}) + \langle \delta P^2 \rangle - 2 \frac{\langle \delta P \delta I \rangle}{\partial I / \partial V S} + \frac{\langle \delta I^2 \rangle}{(\partial I / \partial V S)^2}, \quad (5)$$

where  $\langle \delta V^2 \rangle_{\text{amp}}$  is the noise of the readout amplifier and  $S$  is the responsivity of the detector, which is a function of bias,  $\langle \delta P \rangle$  is the heat flow noise, and  $\langle \delta I \rangle$  is the current noise. The use of strained silicon reduces the constant  $\Sigma$  by a factor of 25 compared to unstrained silicon,<sup>19</sup> this results in a corresponding improvement in the second term of Eq. (5) (the phonon noise).

The other dominant limiting factor to the noise equivalent power will be due to the absorption of photons into the strained silicon. This photon noise term is

$$NEP_{photon}^2 = 2h\nu P_{opt} + \frac{P_{opt}^2}{\delta\nu}, \quad (6)$$

where  $\nu$  and  $P_{opt}$  are the frequency and power of the incident radiation, respectively, and  $\delta\nu$  is the optical bandwidth.

One advantage of the silicon based cold electron bolometer compared to those utilising a metal absorber (SINIS) is that since the tunnel barrier is formed by a Schottky contact, there is no need to fabricate separate insulating layers. The strained silicon cold electron bolometer, studied in this work, consists of three elements: First, the silicon substrate has an epitaxially grown 2.5  $\mu\text{m}$  thick relaxed SiGe (80% silicon) straining layer. On top of the straining layer is a 30 nm thick layer of  $n^{++}$  doped silicon ( $N_D = 4 \times 10^{19} \text{ cm}^{-3}$ ) etched to form a rectangular mesa with an area of  $38 \mu\text{m} \times 14 \mu\text{m}$ . Finally, the top layer is a 100 nm thick film of e-beam evaporated aluminium. This final layer is patterned to form both the contacts to the doped silicon absorber and a twin slot antenna. The contacts to the absorber are both  $30 \mu\text{m} \times 5 \mu\text{m}$  and have a give a tunnelling resistance of 290  $\Omega$ . The twin slot antenna has been designed to couple 160 GHz radiation

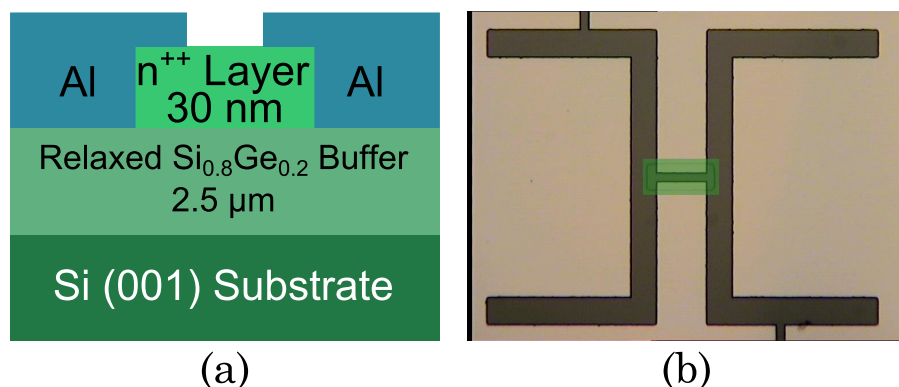


FIG. 2. (a) Cross-sectional view of cold electron bolometer structure. (b) Optical image of a cold electron bolometer. A small island absorber of  $n^{++}$  doped silicon ((a)—green and (b)—highlighted green) sits atop a strained SiGe virtual substrate ((a)—light green and (b)—brown); the top layer of aluminium ((a)—blue and (b)—beige) forms both the antenna structure and the contacts to the absorber; the small slots, which can be seen at the edges of the device, allows DC measure of the cold electron bolometer without affecting the antenna coupling.

to the central absorber and the coupling has been simulated with Ansoft's HFSS software prior to fabrication. The device design is shown in Fig. 2.

A schematic of the testing setup is shown in Fig. 3. The detector was housed in a liquid helium cryostat and cooled to 350 mK using a helium-3 refrigerator. Radiation, visible through a window in the outer cryostat shield, was fed in to a pair of back-to-back horns, the beam from this horn pair was then focussed on to the detector's antenna by a hemispherical silicon lens. This optical coupling scheme was not optimised for high efficiency but designed to minimise stray light coupling to the device.

The detector was current biased using a differential voltage source and a pair of cold 1 M $\Omega$  biasing resistors. The voltage output of the detector was fed into two matched junction field-effect transistor (JFET) differential amplifiers, each of which had an input referred noise of 2 nV Hz $^{-1/2}$ . The output of each of these amplifiers was then passed to a computer which cross-correlated the signal in real time and resulted in a final input referred correlated noise, after averaging, of 300 pV Hz $^{-1/2}$  for the readout system. For optical testing, we used an eccosorb load chopped between 300 K and 77 K.

The silicon cold electron bolometer has been tested both dark and optically loaded. Dark measurements consist of current-voltage (IV) characterisation at various bath (phonon) temperatures. The optical response of the device to a variable temperature blackbody source has also been measured. Fig. 4 compares the current-voltage relationship for the detector in these various conditions; it can be seen that the optically

loaded measurements correspond to higher electron temperature in the device and therefore more linear current-voltage curves compared to the corresponding unloaded measurement. In fact, the optically loaded curves are similar to a dark measurement at a much higher phonon temperature.

From the measured voltage for a given current bias and using Eq. (1), we can calculate the temperature of the electrons. This model, shown as the lines in Fig. 4, shows that a high quality fit to the data (open circles) can be achieved based on this algorithm in all cases. The electron temperatures found from this fit were 570 mK and 640 mK at zero bias for the 77 K and 300 K illuminations. The increase from the phonon temperature of 350 mK is accounted for by the incident power heating the electrons. At a bias corresponding to a voltage of  $\sim 2\Delta$  across the detector, the minimum electron temperatures achieved for the two illumination levels were 350 mK and 500 mK. By use of Eq. (3) at zero bias, combined with the dimensions of the absorbing island and the measured value of  $\Sigma$  ( $2.7 \times 10^7$  WK $^{-6}$  m $^{-3}$ ) and assuming the electron temperature is significantly greater than that of the phonons, we compute the absorbed power to be 10.5 pW and 21.5 pW for the two load temperatures. We believe that there is a contribution of approximately 5 pW from stray light to both of these powers.

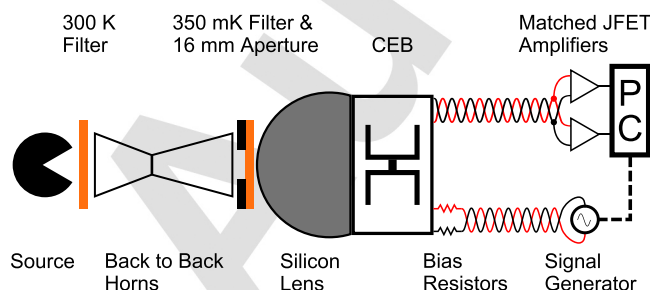


FIG. 3. Experimental setup, radiation is focussed onto the detector chip via a pair of back-to-back horns and a silicon lens. Optical filters are placed before and after the horns and have the effect of limiting the radiation seen by the detector to an upper limit of 300 GHz. The detector is biased via a simple voltage generator and biasing resistors. The voltage output of the detector is sent into two JFET based amplifiers (each with an input referred noise of 2 nV Hz $^{-1/2}$ ) and the output of these is correlated to achieve a final input referred noise of 300 pV Hz $^{-1/2}$ .

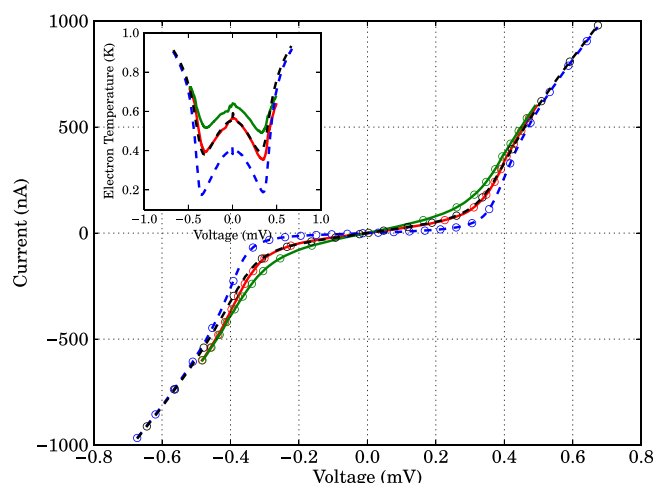


FIG. 4. IV characteristics and model fit. Solid lines optical measurements; dashed lines dark measurements. Red – 77 K source; green – 300 K source; blue –  $T_{ph} = 350$  mK; black –  $T_{ph} = 550$  mK. There is a clear shift of the IV towards the linear as the incident power is increased. Lines—model fit based on  $T_e$  fitting in Eq. (1). Circles—heavily reduced experimental data. Inset—variation in electron temperature with bias; colours as in main figure.



The responsivity, at a particular current bias, of the cold electron bolometer can be calculated from the change in the voltage when the incident power changes by a known amount. From the calculated absorbed powers for the two illuminations and the voltage changes resulting from this change (seen in Fig. 4), we calculate the responsivity to have a maximum of  $7.9 \times 10^6 \text{ V W}^{-1}$  for the 77 K (10.5 pW) source and  $2.8 \times 10^6 \text{ V W}^{-1}$  for the room temperature (21.5 pW) source. In both the cases, the maximum responsivity occurs when the voltage across the device is just below  $2\Delta$ , as is expected. Fig. 5 shows the noise equivalent power calculated from these results. For both the 77 K and the 300 K loading, this is dominated by photon noise. From Fig. 5, we see that the 77 K noise equivalent power is  $1.1 \times 10^{-16} \text{ W Hz}^{-1/2}$ .

The speed of the detector can be found from the roll-off in the white noise level from the photon noise or from measuring the change in responsivity for a modulated signal as a function of frequency. We attempted to measure this using a coherent 150 GHz tunable source which could be chopped on and off at frequencies up to 6 kHz but did not see any reduction in the signal and we also did not see any roll-off in the noise power (as seen in Fig. 5) up to the bandwidth of the readout amplifier (100 kHz). From this, we conclude that the time-constant of this detector is less than  $1 \mu\text{s}$ .

From Eq. (5), we compute that the limit on the electrical (dark) noise equivalent power, for optical loading less than 1 pW, from the electron-phonon interaction is  $8.3 \times 10^{-18} \text{ W Hz}^{-1/2}$ , this compares well to the “dark” noise equivalent power estimations for hot electron bolometer type devices operating at comparable phonon temperatures,<sup>21</sup> which share a common noise limit in these circumstances. The current proof of concept detector has a very large absorbing element, if this was reduced by a factor of 10 (which is still larger than the absorbing element of the comparable hot electron bolometer<sup>21</sup> and still possible with standard photolithography) the phonon noise limit would be reduced to  $2.6 \times 10^{-18} \text{ W Hz}^{-1/2}$  for the same operating temperature.

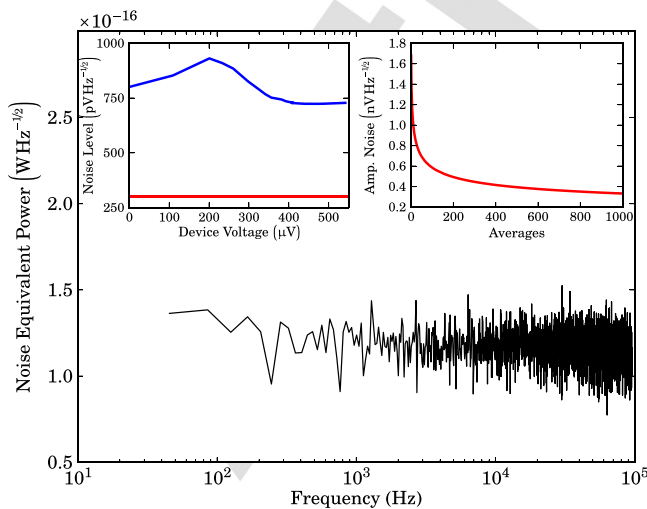


FIG. 5. Noise equivalent power for a SiCEB, as a function of readout frequency, operating at optimum bias ( $eV = 2\Delta$ ) with 10.5 pW of absorbed optical power. Left inset—measured device noise (blue) and amplifier noise limit (red). Right inset—reduction in amplifier noise with averaging for two JFET amplifiers operating in cross-correlated mode.

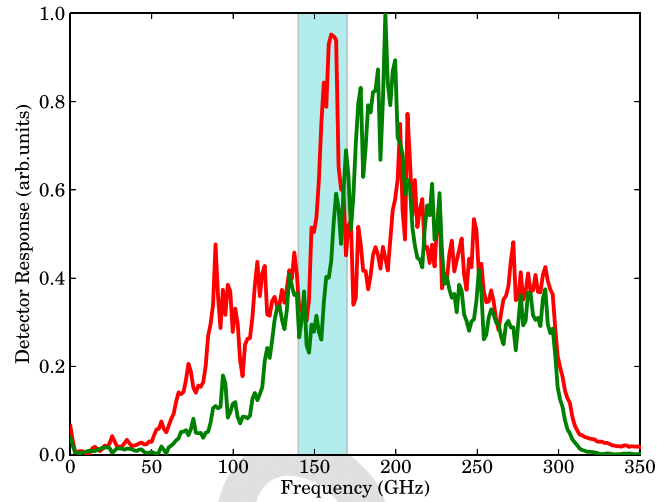


FIG. 6. Response of the strained silicon cold electron bolometer to a Fourier transform spectrometer with a mercury arc lamp source. Red—response to a vertically polarised source; green—horizontally polarised source; highlighted region—expected frequency range of the antenna’s 3 dB response.

We have also measured the response of the strained silicon cold electron bolometer as a function of the frequency of incident radiation. This was performed in both linear polarisations; since the detector used a twin-slot antenna to couple radiation, it was expected that there would be more response in one polarisation. The measured spectral response is shown in Fig. 6. The measured response has a cutoff of 300 GHz due to the optical filters in place. The highlighted region denotes the expected frequency range of the twin-slot antenna. There is a clear excess response in this region in the vertical polarisation, parallel to the twin slot antenna. The peak in the horizontal polarisation may be attributed to response in the coplanar waveguide (CPW), which couples radiation to the absorber and is also due to the cuts in the aluminium (seen in Fig. 2(b)), which break the DC continuity around the detector. Both these cuts and the coplanar waveguide are orthogonal to the twin-slot antenna. The plateau level, around half of the maximum response, is due to a combination of photons directly splitting Cooper pairs in the aluminium along with direct absorption in the doped silicon mesa, general broadening of the absorption spectrum due to the silicon lens and the integrating cavity in which the detector was housed.

We have demonstrated a detector that utilises direct electron cooling via Schottky tunnelling contacts between aluminium and strained silicon. We have shown that this detector has a photon noise limited noise equivalent power of  $1.1 \times 10^{-16} \text{ W Hz}^{-1/2}$  when observing a 77 K blackbody and under low optical loading conditions has an electrical or dark noise equivalent power, at 350 mK, of  $8.3 \times 10^{-18} \text{ W Hz}^{-1/2}$ . The time constant of this detector has been determined to be less than  $1 \mu\text{s}$ , which compares extremely favourably to other detector types with similar noise equivalent power.

This work has been financially supported by the EPSRC through Grant No. EP/F040784/1.

<sup>1</sup>D. Morozov, P. Mauskopf, P. Ade, M. Ridder, P. Khosropanah, M. Bruijn, J. Van der Kuur, H. Hoevers, J. Gao, and D. Griffin, *IEEE Trans. Appl. Supercond.* **21**, 188 (2011).

- <sup>2</sup>S. Doyle, P. Mauskopf, J. Naylon, A. Porch, and C. Duncombe, *J. Low Temp. Phys.* **151**, 530 (2008).
- <sup>3</sup>M. Nahum, P. Richards, and C. Mears, *IEEE Trans. Appl. Supercond.* **3**, 2124 (1993).
- <sup>4</sup>M. Nahum, T. M. Eiles, and J. M. Martinis, *Appl. Phys. Lett.* **65**, 3123 (1994).
- <sup>5</sup>D. R. Schmidt, K. W. Lehnert, A. M. Clark, W. D. Duncan, K. D. Irwin, N. Miller, and J. N. Ullom, *Appl. Phys. Lett.* **86**, ■ (2005).
- <sup>6</sup>R. Leoni, *New Astron. Rev.* **43**, 317 (1999).
- <sup>7</sup>J. T. Muhonen, M. J. Prest, M. Prunnila, D. Gunnarsson, V. A. Shah, A. Dobbie, M. Myronov, R. J. H. Morris, T. E. Whall, E. H. C. Parker, and D. R. Leadley, *Appl. Phys. Lett.* **98**, ■ (2011).
- <sup>8</sup>E. Otto, M. Tarasov, P. K. Grimes, A. Chekushkin, L. S. Kuzmin, and G. Yassin, *Supercond. Sci. Technol.* **26**, 085020 (2013).
- <sup>9</sup>M. Tarasov, L. Kuzmin, V. Edelman, S. Mahashabde, and P. De Bernardis, *IEEE Trans. Appl. Supercond.* **21**, 3635 (2011).
- <sup>10</sup>J. Pekola, *Nature* **435**, 889 (2005).
- <sup>11</sup>M. M. Leivo, J. P. Pekola, and D. V. Averin, *Appl. Phys. Lett.* **68**, 1996 (1996).
- <sup>12</sup>A. M. Savin, M. Prunnila, P. P. Kivinen, J. P. Pekola, J. Ahopelto, and A. J. Manninen, *Appl. Phys. Lett.* **79**, 1471 (2001).
- <sup>13</sup>J. P. Pekola, T. T. Heikkilä, A. M. Savin, J. T. Flyktman, F. Giazotto, and F. W. J. Hekking, *Phys. Rev. Lett.* **92**, 056804 (2004).
- <sup>14</sup>P. D. Mauskopf, J. J. Bock, H. D. Castillo, W. L. Holzapfel, and A. E. Lange, *Appl. Opt.* **36**, 765 (1997).
- <sup>15</sup>M. D. Audley, G. de Lange, J.-R. Gao, P. Khosropanah, M. Ridder, L. Ferrari, W. M. Laauwen, M. Ranjan, P. D. Mauskopf, D. Morozov, and N. A. Trappe, *Proc. SPIE* **8452**, 84520B (2012).
- <sup>16</sup>W. S. Holland, D. Bintley, E. L. Chapin, and A. Chrysostomou, *Mon. Not. R. Astron. Soc.* **430**, 2513 (2013).
- <sup>17</sup>L. Kuzmin, *Infrared and Millimeter Waves* (■, 2004), pp. 239–240.
- <sup>18</sup>B. D. Jackson, P. A. J. De Korte, J. Van der Kuur, P. Mauskopf, J. Beyer, M. Bruijn, A. Cros, J. Gao, D. Griffin, R. Den Hartog, M. Kiviranta, G. De Lange, B. van Leeuwen, C. Macculi, L. Ravera, N. Trappe, H. Van Weers, and S. Withington, *IEEE Trans. THz Sci. Technol.* **2**, 12 (2012).
- <sup>19</sup>M. J. Prest, J. T. Muhonen, M. Prunnila, D. Gunnarsson, V. A. Shah, J. S. Richardson-Bullock, A. Dobbie, M. Myronov, R. J. H. Morris, T. E. Whall, E. H. C. Parker, and D. R. Leadley, *Appl. Phys. Lett.* **99**, 251908 (2011).
- <sup>20</sup>D. Golubev and L. Kuzmin, *Appl. Phys. Lett.* **89**, 6464 (2001).
- <sup>21</sup>B. S. Karasik and R. Cantor, *Appl. Phys. Lett.* **98**, ■ (2011).

AQ2

AQ5  
AQ3